

THE QUEST RR LYRAE SURVEY. I. THE FIRST CATALOG¹

A. K. VIVAS,^{2,3} R. ZINN,³ C. ABAD,² P. ANDREWS,⁴ C. BAILYN,³ C. BALTAY,⁴ A. BONGIOVANNI,² C. BRICEÑO,² G. BRUZUAL,² P. COPPI,^{3,4} F. DELLA PRUGNA,² N. ELLMAN,⁴ I. FERRÍN,⁵ M. GEBHARD,⁶ T. GIRARD,³ J. HERNANDEZ,^{2,5} D. HERRERA,⁴ R. HONEYCUTT,⁶ G. MAGRIS,² S. MUFSON,⁶ J. MUSSER,⁶ O. NARANJO,⁵ D. RABINOWITZ,⁴ A. RENGSTORF,⁶ P. ROSENZWEIG,⁵ GE. SÁNCHEZ,² GU. SÁNCHEZ,² B. SCHAEFER,⁷ H. SCHENNER,² J. A. SNYDER,^{4,3} S. SOFIA,³ J. STOCK,² W. VAN ALTENA,³ B. VICENTE,² AND K. VIEIRA³

Received 2003 May 22; accepted 2003 October 16

ABSTRACT

With the 1 m Schmidt telescope of the Llano del Hato Observatory and the QUEST CCD camera, 380 deg² of the sky have been surveyed for RR Lyrae variables in a band 2^h3 wide in declination (centered at $\delta = -1^\circ$) and covering right ascensions from 4^h1 to 6^h1 and from 8^h0 to 17^h0. The bright limit (due to CCD saturation) and the faint limit are $V \sim 13.5$ and ~ 19.7 , respectively, which correspond to ~ 4 and ~ 60 kpc from the Sun. We present a catalog of the positions, amplitudes, mean magnitudes, periods, and light curves of the 498 RR Lyrae variables that have been identified in this region of the sky. The majority of these stars (86%) are new discoveries. The completeness of the survey has been estimated from simulations that model the periods and light curves of real RR Lyrae variables and take into account the pattern of epochs of observation. While the completeness of the survey varies with apparent magnitude and with position, almost everywhere in the surveyed region it is quite high ($>80\%$) for the type *ab* RR Lyrae variables and between 30% and 90% for the low-amplitude type *c* variables.

Key words: Galaxy: halo — stars: variables: other — surveys

On-line material: machine-readable table

1. INTRODUCTION

Recent surveys of the spatial distribution and the kinematics of the halo stars have provided very strong evidence that the accretion of satellite galaxies has played a major role in the formation of the halo and possibly the whole Milky Way (Majewski et al. 2003; Newberg et al. 2002; Vivas et al. 2001; Dohm-Palmer et al. 2001; Ibata et al. 2001b; Yanny et al. 2000; Ivezić et al. 2000). The most vivid evidence is provided by the Sagittarius dwarf spheroidal (dSph) galaxy and the long streams of stars emanating from this tidally disrupted satellite. There are in addition several other recently discovered features in the halo that may be the debris of ancient mergers of low-mass galaxies with the Milky Way (Yanny et al. 2003; Vivas & Zinn 2003, 2004; Newberg et al. 2002), and the characteristics of the thick disk population suggest that it formed when a relatively massive satellite galaxy merged with the Milky Way and “puffed up” a preexisting thin disk population (Gilmore, Wyse, & Norris 2002). The recent discoveries of what appear to be tidal streams in the halo of M31 and more distant galaxies indicate that this is a wide-spread phenomenon (Ibata et al. 2001a; Peng et al. 2002).

In light of these recent developments, one is tempted to conclude that the halos of galaxies are formed only by accretion. During the long debate over whether the halo formed during the rapid collapse of a large gas cloud (Eggen, Lynden-Bell, & Sandage 1962) or more slowly through the merger of satellite galaxies (Searle & Zinn 1978), several authors argued that the data on the halo stars and the globular clusters pointed to a combination of the two pictures (Chiba & Beers 2001; Norris 1994; Zinn 1993; Majewski 1993). The data for the outer halo (galactocentric radius, R_{gal} , >8 kpc) appear to be consistent with the accretion of satellites, while some features of the inner halo, such as its significant prograde rotation, are suggestive of a collapse picture. It is clearly important to determine the properties of the halo in greater detail, particularly as functions of R_{gal} and distance from the Galactic plane, and to discover any additional tidal streams from disrupted satellites.

Another motivation for surveying the halo comes from recent theoretical models of the growth of galaxies in the popular cold dark matter (CDM) cosmology. According to these models, galaxies similar to Milky Way formed through the merger of a large number of dark matter subhalos, some of which contained gas and formed stars prior to their disruption and incorporation into the nascent Milky Way. The stars that formed in these subhalos, which resembled dwarf galaxies, are predicted to be part of today’s stellar halo. This theoretical picture appears to be in good agreement with the recent discoveries of the substructure in the halo mentioned above, with, however, one exception. The theoretical models predict the formation of such a large number of dark matter subhalos that even after the merger of many to make the Milky Way, several hundred should be orbiting the Milky Way today. This apparent inconsistency with the number of known satellite galaxies, which has become known as the satellite problem of CDM cosmology, may be a sign that the theoretical models need substantial revision (Freeman & Bland-Hawthorn 2002

¹ Based on observations collected at the 1 m Schmidt Telescope of the Llano del Hato Observatory, Venezuela.

² Centro de Investigaciones de Astronomía, Apdo. Postal 264, Mérida 5101-A, Venezuela; akvivas@cida.ve.

³ Department of Astronomy, Yale University, P.O. Box 208101, New Haven, CT 06520-8101.

⁴ Department of Physics, Yale University, P.O. Box 208120, New Haven, CT 06520-8120.

⁵ Departamento de Física, Universidad de Los Andes, Mérida 5101, Venezuela.

⁶ Department of Astronomy, Indiana University, 319 Swain West, Bloomington, IN 47405.

⁷ Department of Astronomy, University of Texas at Austin, Austin, TX 78712.

and references therein). It also points out the importance of documenting in as much detail as possible the merger history of the Milky Way and of searching the halo for stellar systems that might be subhalos that contain a relatively small number of stars.

This paper is the first of series that discusses the results that have been obtained from a survey for RR Lyrae variable stars (hereafter RRLSs) in the Galactic halo. RRLSs are easily recognized by their characteristic light curves, periods, and colors. Most importantly, their luminosities span a narrow range and are quite bright compared with most other types of halo stars. Consequently, their spatial distribution is easily determined from their apparent magnitudes, and they can be observed over large distances in the halo. These characteristics, which make RRLSs superb probes of the halo, have been recognized for decades, and studies of RRLSs have provided much of our present knowledge of the structure, kinematics, and the metal abundance distribution of the halo (see § 1.1). There are, however, a few disadvantages of RRLSs as probes that must be mentioned. Because RRLSs are horizontal-branch (HB) stars that lie in the instability strip, they only occur in very old stellar populations (>8 Gyr). From studies of the color-magnitude diagrams of globular clusters, it is known that the frequency of RRLSs in an old population depends on its metal abundance (the first parameter affecting HB morphology) and a second parameter, most likely age, that changes HB morphology at constant metallicity (see Rey et al. 2001; Catelan et al. 2001a; Catelan, Ferraro, & Rood 2001b, for recent discussions). Age and metallicity and perhaps other factors, if age is not the only second parameter, must be within certain broad ranges to produce RRLSs. While it is easy to think of stellar populations that a survey for RRLSs would fail to detect because of these limitations, such as a galaxy containing very few old stars or one whose old stars were only metal-rich, real galaxies are unlikely to have these characteristics and to be completely devoid of these stars. Indeed, RRLSs are found in large numbers in all of the old stellar populations of the Milky Way (halo, thick disk, and bulge) and in every one of the dwarf galaxies that orbit the Milky Way. Since the Sloan Digital Sky Survey (SDSS) for RRLSs

(Ivezic et al. 2000) and the first part of our survey (Vivas et al. 2001) detected the tidal stream from the Sagittarius dSph galaxy and other density enhancements in the halo that may be other tidal streams, it is clear that RRLS surveys do provide useful information on the merger history of the Milky Way.

In this paper we present a catalog of RRLSs that lie in the first strip of the sky to be surveyed with the 1 m Schmidt telescope of the Llano del Hato Observatory and the QUEST⁸ CCD camera. In the next subsection we summarize the previous large-scale surveys for RRLSs. We describe the observations and basic data reduction in § 2. The selection of variable stars and identification of RRLSs is explained in § 3. In § 4 we present a catalog of 498 RRLSs and discuss the completeness of the survey and possible contaminants. Section 5 contains a summary of the survey. Subsequent papers will discuss the spatial distribution of the RRLSs, the pulsational properties of the RRLSs and spectroscopic measurements of the metal abundances and the radial velocities of some of the stars.

1.1. Previous Surveys

Since RRLSs have been used many times in the past to probe the Milky Way, it is important to compare the QUEST survey with the previous large-scale ones. This is done in Table 1, where the maximum distance from the Sun, r , was calculated from the faint limiting magnitude of the survey. Many of the previous surveys were made with photographic plates and in specific directions in the Galaxy, mainly the north Galactic pole (NGP), the Galactic center (GC), or the anticenter direction (GAC). Each survey has a different degree of completeness, which may vary with position on the sky, as indeed it does for the QUEST survey (see § 4.1). The QUEST survey represents an advance in amount of area of the sky covered to a large limiting distance. Its average completeness for type *ab* RRLSs, greater than 80% in most regions, is competitive with the best and better than some (e.g., the deeper SDSS survey is only $\sim 30\%$ complete; see § 4.2).

⁸ QUEST stands for Quasar Equatorial Survey Team (see § 2.1).

TABLE 1
SURVEYS OF RR LYRAE STARS IN THE HALO

Survey	Area (deg ²)	r (kpc)	Galactic Coordinates	Comments
Lick ^a	200	~ 25	NGP, GC	Photographic
Palomar-Groningen ^b	95	~ 30	GC	Photographic
Hawkins ^c	16	~ 120	Intermediate Gal. lat.	Photographic
Saha ^d	130	~ 60	Intermediate Gal. lat. and GAC	Photographic
CTI ^e	36	~ 30	Multiple	
SDSS ^f	100	~ 120	High Gal. lat.	Only candidate RRLSs
ROTSE ^g	2300	~ 7	Multiple	
QUEST ^h	380	~ 60	Multiple	

^a Kinman, Wirtanen, & Janes 1965; Kinman, Wirtanen, & Janes 1966; Kinman, Mahaffey, & Wirtanen 1982; Kinman et al. 1984.

^b Plaut 1966; Plaut 1968; Plaut 1971.

^c Hawkins 1984.

^d Saha 1985.

^e Wetterer et al. 1996.

^f Ivezic et al. 2000.

^g Akerlof et al. 2000.

^h This work.

2. OBSERVATIONS AND DATA REDUCTION

2.1. The *QUEST* Camera

The survey was carried out with the *QUEST* camera, which is a 16-chip CCD mosaic detector installed at the 1 m (clear aperture) Schmidt telescope at Llano del Hato Observatory in Venezuela, located at 3610 m elevation, close to the equator ($8^{\circ}47'$ north) and under very dark skies. This camera has been built by the *QUEST* collaboration, which includes Yale University, Indiana University, Centro de Investigaciones de Astronomía (CIDA), and Universidad de Los Andes. The main goal of *QUEST* is to perform a large-scale survey of quasars, but its impressive capabilities can be used for other kinds of surveys. For a detailed description of the instrument, see Baltay et al. (2002). We describe here the properties that are most relevant to our survey for RRLSs.

The 16 2048×2048 Loral CCD devices are set in a 4×4 array, covering most of the focal plane of the Schmidt telescope. The chips are front illuminated and have been coated to enhance their UV response. The pixel size of $15 \mu\text{m}$ corresponds to a scale of $1''.02 \text{ pixel}^{-1}$. The entire camera has a field of view of $2''.3 \times 2''.3$, with small gaps between CCDs (a few arcminutes).

The camera has been designed for observing in drift-scan mode: the telescope is fixed and the CCDs are read out east-to-west at the sidereal rate as stars drift across the device. This procedure results in the generation of a continuous strip (or “scan”) of the sky, $2''.3$ wide at constant declination. In addition to its high efficiency for covering large areas in a short time, drift-scanning offers other significant advantages. The telescope does not have to be moved, and there is no observing time lost during the reading out of the CCDs. Flat-fielding errors are minimized since each stellar image is obtained by averaging over many pixels as it travels over the CCD, and astrometric precision is enhanced because the zenith angle is constant throughout a scan. One of the limitations of drift-scanning is that the sky motion is only parallel to the CCDs on the equator and the rate of drift on the focal plane is a strong function of the declination. To compensate for this effect, each row of CCDs is mounted on a separate “finger,” which pivots at one end, allowing the row to be independently aligned perpendicular to the star paths. In addition, the chips are clocked out at separate rates corresponding to the change in sidereal rate as a function of δ . Even so, the size of the device and the image scale limit the declination range available for drift-scanning. In order to limit image smearing to ≤ 0.5 pixels, drift-scanning is restricted to $-6^{\circ} \leq \delta \leq +6^{\circ}$.

The drift-scan mode allows us to obtain quasi-simultaneous multiband photometry since each finger can be fitted with separate filters. Stars will successively cross over four chips in a column, each with its own filter. Several filter sets are available, which include *UBVRI* and $H\alpha$. One can then survey huge areas on the sky in a very efficient way, at a rate of $34 \text{ deg}^2 \text{ hr}^{-1} \text{ filter}^{-1}$.

The exposure times (hence the limiting magnitude) are set by the time a star takes to cross a single chip (140 s at $\delta = 0^{\circ}$). The limiting magnitude for useful photometry is $V \approx 19.5$ ($S/N = 10$). Saturation occurs at $V = 13.0$ – 14.5 depending on the CCD, since they have different well capacities.

The data acquisition system, which is able to handle ~ 30 gigabytes of raw data per night, is described in Sabbey, Coppi, & Oemler (1998). Instead of creating a single, very long image,

the scan is divided in frames, usually 2048 pixels long each, which are much more manageable.

2.2. The Data

This survey uses drift-scan observations of the same region of the sky taken with the *QUEST* camera over a 2.3 yr period, from 1998 December to 2001 April. The observations were designed for different scientific purposes, and thus the time spacing and filter set used varies. There were four different sequences of filters, *UBUV*, *RBRV*, *RBIV*, and *RH α IV*. Because *V* observations were obtained on each of the nights, they were chosen for the search for RRLSs. Although the amplitude of RRLSs is largest in the *B* band (hence, they should be easier to detect in that filter), the low sensitivity of the CCDs at short wavelengths make the *V* observations more efficient to pick up distant RRLSs. The limiting magnitude in *B* is ~ 18.5 , which corresponds to detecting RRLSs up to a distance of $\sim 40 \text{ kpc}$, significantly closer than what we can find using the *V* band.

The scans have a constant declination, covering from $-2^{\circ}20'$ to $+0^{\circ}01'$, with three small gaps that separate the four columns of CCDs. In right ascension, they cover from $4^{\text{h}}1$ to $6^{\text{h}}1$ and from 8^{h} to 17^{h} . We intentionally left out the region between 6^{h} and 8^{h} to avoid the crowding and extinction problems of very low Galactic latitudes. Thus, we have two strips of the sky, 30° and 135° long, respectively, each $2''.13$ wide, for a total coverage of 380 deg^2 of the sky. The strips cover a large range of Galactic latitude (Fig. 1), from $|b| = 10^{\circ}$ to 63° .

The general observational strategy was to point the telescope to the meridian and scan all night. To avoid the Galactic plane or scattered moon light, some of the scans were started at a different hour angle (always $< 2^{\text{h}}5$). On a few occasions, the same region of the sky was scanned twice during the same night. The length and start time of the scans were frequently determined by clouds. Thus, the time separation between scans goes from a few hours, to days, weeks, and years. This irregular spacing of the observations removes some of the

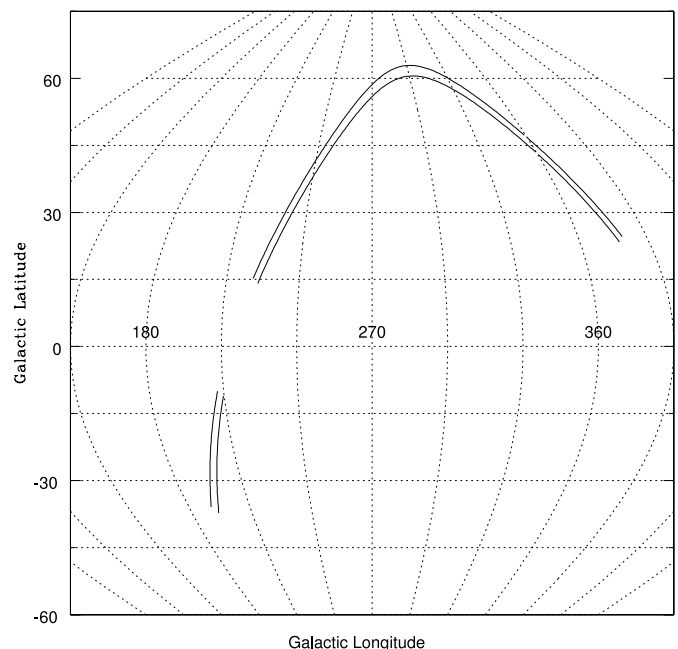


Fig. 1.—Galactic coordinates of the region of the survey

aliasing in our period search. Figure 2 shows the time spacing and range of right ascension covered by each scan. As a result, the time spacing and total number of observations varies over the sky. We collected 112 scans during 96 nights, for a total of 467.5 hr of observation (1.7 terabytes of data). There are 15–40 scans along each line of sight. The most observations were collected during the month of March of each year, which is partly a consequence of the weather patterns at the Llano del Hato Observatory.

Seeing varied from $2''.1$ to $3''.6$, with a mean value of $2''.7$. Given the size of the camera pixels, undersampling is not a problem.

2.3. The Photometry Pipeline

Each scan of the sky was reduced with the standard QUEST software. This automated process, which requires very little interaction with the user, produces a catalog of positions and instrumental magnitudes for all objects.

The software first performs the basic reductions, bias subtraction, and flat fielding in the north-south direction. Then, objects are detected in all 16 chips. This is done in the standard way by selecting objects above a threshold over the local (each frame) background, with, however, no provision for deblending close objects. These lists of thousands of objects are used to find precise transformations of the position of objects in a reference chip to the other three chips, which have observed the same field but in different filters. Usually, R or V are chosen as the reference chip because the signal-to-noise ratio is higher in these bands. Aperture photometry is performed on the objects detected in the reference chip and at the positions calculated to be the positions of the objects in the other three chips. This minimizes centering problems for faint objects in the less efficient filters. It also guarantees that for each object, we will have measurements in all four bands. The aperture radius is set at $1 \times \text{FWHM}$, where the seeing is

determined using all bright, nonsaturated stars in each individual frame. This small aperture was chosen to reduce photometric errors in the faintest stars. Finally, the astrometry is done by matching all objects with the USNO-A2.0 catalog (Monet et al. 1998). The positions have precisions of $\pm 0''.2$. The resulting catalog is stored in binary format. Each object contains a whole set of properties (magnitudes, errors, FWHM, position, shape parameters, etc.) and flags (bad columns, saturation, edge, etc.) that help to eliminate bad measurements and/or false detections.

2.4. Calibration

Near the celestial equator there are sequences of standard stars that have been set up by Landolt (1983), but most of these stars are saturated in our observations. Since our scans are not centered exactly in the celestial equator, the non-saturated standards lie only in the two northernmost rows of CCDs. Consequently, it was necessary to obtain secondary standards.

Observations for the secondary standard fields were made at the YALO (Yale Aura Lisbon Ohio) telescope at Cerro Tololo Inter-American Observatory (Chile) during seven nights in 2000 February. The detector was a 2048×2048 Loral CCD with a field of view of $10'.2 \times 10'.2$. We took fields every 1 hr in right ascension, from $10^{\text{h}}.5$ to $15^{\text{h}}.5$, and at four different declinations, corresponding to each row of CCDs of the QUEST camera. Each night several Landolt fields were also taken. The reduction and aperture photometry of these fields were performed using standard IRAF⁹ routines. A total of 134 secondary standards were set up. Only one YALO observation was obtained for each of these stars. They were checked for variability using our QUEST data, and the stars selected as secondary standards do not show signs of variability over the 2.3 yr baseline of our observations. In addition, we also used 23 nonsaturated Landolt standards that lie in our observed region.

The secondary standards have V magnitudes between 13.0 to 17.6 and span a range of colors $-0.13 < V-R < 1.02$. About 40% of them have colors in the same range as RRLSs ($V-R < 0.42$; see § 3.1). A catalog of secondary standards of this and other regions observed by QUEST will be presented in a forthcoming paper.

A photometric QUEST night, which was used as the reference scan in our search for variables, was calibrated in V and Cousin R , R_C , using these secondary stars. Every row of CCDs was calibrated separately. Very good transformations were obtained to the standard system, with mean rms of 0.02 mag in both filters.

The smaller strip of data that covers the region from 4^{h} to 6^{h} in right ascension was calibrated in a different way. In this case, we took Landolt standard fields with the same QUEST camera for each row of CCDs and at different air masses. The QUEST data in this region were calibrated in the filters V and I_C , with errors in the zero points of 0.03 mag.

3. VARIABLE STARS

Differential photometry has been used to identify the variable stars. After matching by position the stars in a reference scan to all other ones, we obtained a list of 1,264,962 stars that

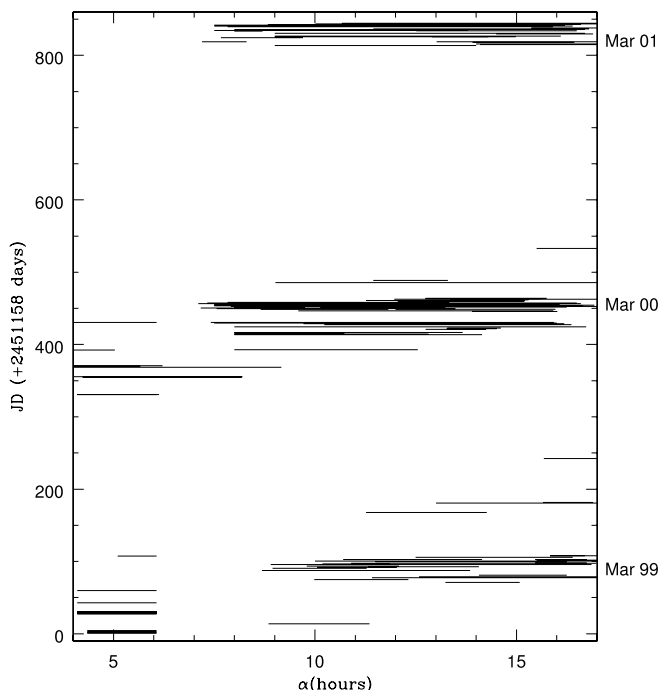


FIG. 2.—Time spacing of the drift-scan observations. Each line represents one scan covering a range in right ascension. At this declination ($\delta = -1^\circ$) the Galactic plane is at $\alpha = 6^{\text{h}}.9$.

⁹ IRAF is distributed by the National Optical Astronomy Observatory, which is operated by the Association of Universities for Research in Astronomy, Inc., under cooperative agreement with the National Science Foundation.

have a minimum of three good measurements. To be considered a match in position, the differences between the reference scan and the others had to be within a radius of less than $2''$.

The instrumental magnitudes were normalized to a reference scan in order to remove variable atmospheric extinction due to differences in air mass and transparency. This normalization to reference magnitudes was made in bins of 0.25° of right ascension, which is equivalent to ~ 1 minute of time in drift-scan mode. For the stars in each bin of right ascension, the differences in magnitude between the scan and the reference scan were calculated, and an ensemble clipped mean was iteratively produced. Given that each bin contains typically several hundred stars, this produces a robust estimate of the zero-point difference between each scan and the reference one. For each star the zero-point differences are subtracted by interpolating among the values of neighbor bins. Figure 3 illustrates an example of this process; the top panel shows the original difference in V magnitudes between a scan and the reference one, and the corrected values are shown in the bottom panel. Notice how the effects of a cloud that was causing an extinction of ~ 0.5 mag at $\alpha = 15^{\text{h}}7$ is eliminated. This part of the process is interactive, and the user can check the corrections and eliminate parts of the scans if not satisfied. In general, we could correct for clouds that caused extinctions of up to 1 mag and thus make use of data taken under mediocre atmospheric conditions.

Because a large number of stars have been observed, the random errors of the differential magnitudes are well determined. These amount to ~ 0.02 mag for $V \leq 17$ but climb to ~ 0.1 mag at $V = 19.5$ as photon statistics dominate the noise. Figure 4 shows the dispersion in the normalized instrumental V magnitudes in one CCD for a 1 hr long piece of a scan (8 deg^2) containing $\sim 35,500$ stars. Each point represents the statistics of 25–30 measurements. Most objects are non-variable and populate the curved region; points above the curve are likely variable stars.

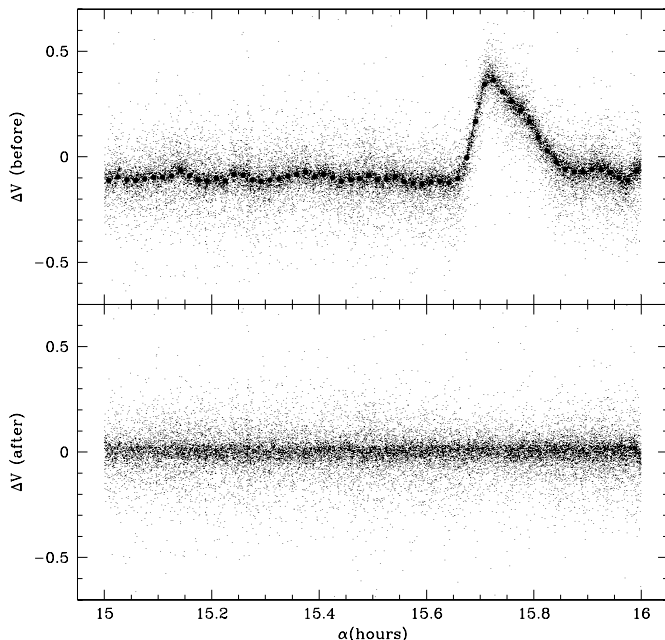


FIG. 3.—Example of the normalization process. Each point represents a star. The plot shows the difference in magnitude between two scans before and after the correction. The dots in the top panel are the mean values of the zero-point difference in each bin.

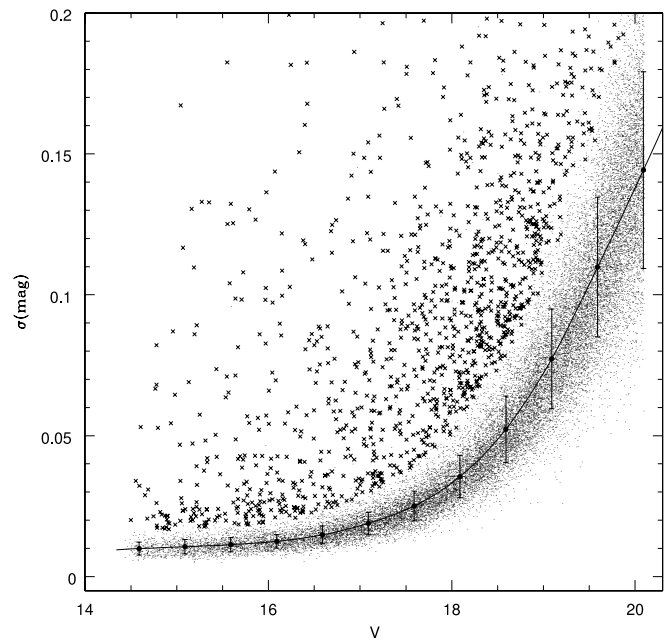


FIG. 4.—The 1σ dispersion in V magnitudes in a 8 deg^2 portion of the QUEST data set of 35,000 stars. The dots are the mean value of the dispersion in bins of 0.5 mag; a clipped mean was used to eliminate variable objects in each bin. Error bars show the 1σ dispersion of the nonvariables in each bin. The fitted line represents then the typical error of our data. Crosses indicate the stars selected as variable by the χ^2 test.

We applied a χ^2 test on the normalized magnitudes to select variable stars (e.g., Saha & Hoessel 1990; Wetterer & McGraw 1996), which is appropriate because nonvariable stars follow a Gaussian distribution of errors. This is illustrated in Figure 5. The χ^2 test gives the probability that the observed spread in magnitude for an object is caused by errors alone. If the probability is very small (≤ 0.01), the object is flagged as variable.

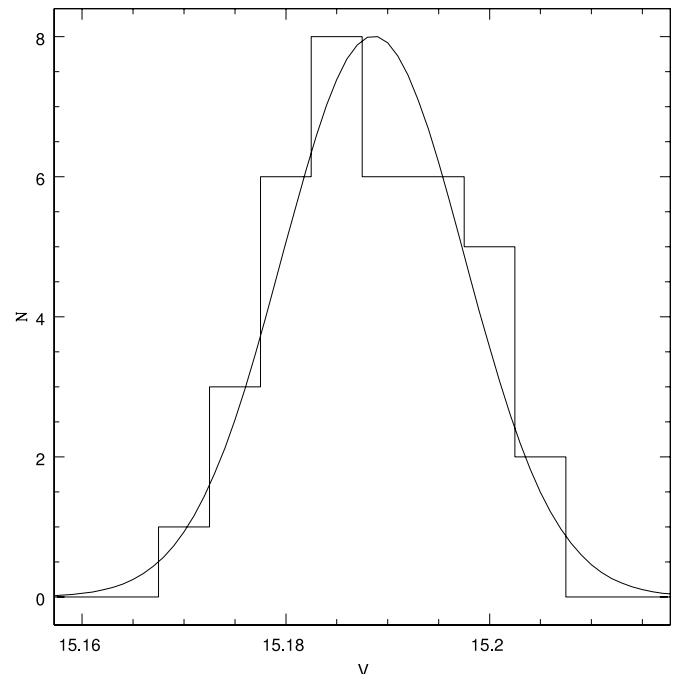


FIG. 5.—Histogram of the distribution of the measurements of a typical, well-observed ($N = 37$), nonvariable star. It is consistent with a Gaussian distribution (curve).

The reduced χ^2_ν is given by

$$\chi^2_\nu = \sum_{i=1}^N \frac{(m_i - \bar{m})^2}{\nu \sigma_i^2}, \quad (1)$$

where m_1, \dots, m_N are the individual magnitudes of a star and \bar{m} is its mean magnitude; $\nu = N - 1$ is the degrees of freedom and σ_i is the error associated with m_i and is taken from the fitted curve shown in Figure 4. The probability distribution function for χ^2_ν , $P(\chi^2_\nu)$, was calculated using standard numerical prescriptions (Press et al. 1992).

Before running the χ^2 test, we eliminated measurements that are potentially affected by a cosmic ray by deleting any point that was more than 4σ away from the mean magnitude for that star. Although this step could affect the detection of genuine variables such as flare stars, we do not expect such behavior in RRLSs, and it is indeed a necessary step to be done before attempting to calculate periods.

We flagged all objects with a 99% confidence level of being variable [$P(\chi^2_\nu) \leq 0.01$]. Given the large number of stars in our sample, this confidence level still flagged about 12,000 objects that are not actually variable. However, to apply a higher confidence level would reject some real yet low-amplitude variables. Additional constraints were used to isolate the RRLSs. The minimum amplitude of the variation that we could detect depended on the magnitude of the star. The final list of potential variable stars contained 72,082 objects, or 5.7% of the initial sample. This percentage is somewhat larger than those found by other variability surveys, e.g., 0.2%–2% in the Flagstaff Astrometric Scanning Transit Telescope (FASTT, Henden & Stone 1998); 0.8% in the ROTSE variability survey (Akerlof et al. 2000). As explained by Henden & Stone (1998), many false variables could appear because of close neighbors or blended objects. We did not try to identify these false variables because nearly none would pass our next criteria for selecting RRLSs (see below).

While our strategy for identifying variable stars specifically targeted RRLSs, our list contains many other types of variables that are important to different fields of astronomy. For example, this same list of variables is being used to search for T Tauri stars with high success (Briceño et al. 2001). There are only 50 stars fainter than $V = 14$ listed in the Combined General Catalog of Variable Stars (GCVS, Kholopov et al. 1998) in this region of the sky, and the faintest one is only magnitude 16.6. A database with the complete list of variables is in preparation.

Since we may have missed some objects that the photometry pipeline flagged as bad measurements in the first reference scan, we repeated the whole process using a different scan as reference and included the new variables in the list. This was especially important for recovering objects that happened to lie in bad columns in the first reference scan.

3.1. RR Lyrae Star Identification

The RRLSs were identified by their color, amplitude, period and the shape of the light curve. Because RRLSs are HB stars that lie in the instability strip ($6100 \leq T_{\text{eff}} \leq 7400$ K; Smith 1995), the number of candidates can be greatly reduced by imposing a limit in the color of the stars, especially on the red side of the distribution. We used the color $V-R_C$ instead of $(B-V)$ because the R observations are numerous and go as deep as V , which is not the case for B . RRLSs change their effective temperature during the pulsation cycle,

and are bluer at maximum light than at minimum. Since we calculate the mean colors of our stars from a large number of observations in both V and R , they should be close to the true mean color of the star. A HB star with temperature of 6000 K has a color $V-R_C = 0.30$ (Lejeune, Cuisinier, & Buser 1998). Over most of the region of the sky observed in this survey, the color excess, $E(V-R_C)$, is less than 0.02 (Schlegel, Finkbeiner, & Davis 1998). Allowing for a maximum observational error of 0.1 mag, we rejected all variables with $V-R_C > 0.42$ from our list of candidate RRLSs. This limit was increased to 0.50 in regions near the Galactic plane, where $E(V-R_C)$ can be as high as 0.10. We tested higher values of the color limit in small regions of sky and did not find any additional stars that are definitely RRLSs. Figure 6 shows a color-magnitude diagram of a small part of the sky; the RRLSs found here (triangles) lie well to the left of the limit of $V-R_C = 0.42$. This figure also illustrates how the number of RRLS candidates is greatly reduced by this color selection. A special case is the region at $\alpha = 5^{\text{h}}2$ to 6^{h} , which approaches to the Galactic plane and contains dense molecular clouds with extinctions of up to a few magnitudes. We do not expect the sample to be complete in this region.

Another constraint was made in the amplitude of the variables since RRLSs have well known range of variations [$\Delta V = 0.2$ – 0.7 mag for type c (RRc) and 0.4 – 1.6 mag for type ab (RRab)]. We only determined the period if the variable had 12 or more V observations. Sometimes less than 12 data points are sufficient to calculate a period, while depending on the phase coverage, other times it can be too few. However, we introduced this limit in the minimum number of observations based on our experience and for the sole purpose of automating the process as much as possible.

The final selection criteria involved calculating the periods and examining the resulting light curves. Periods were

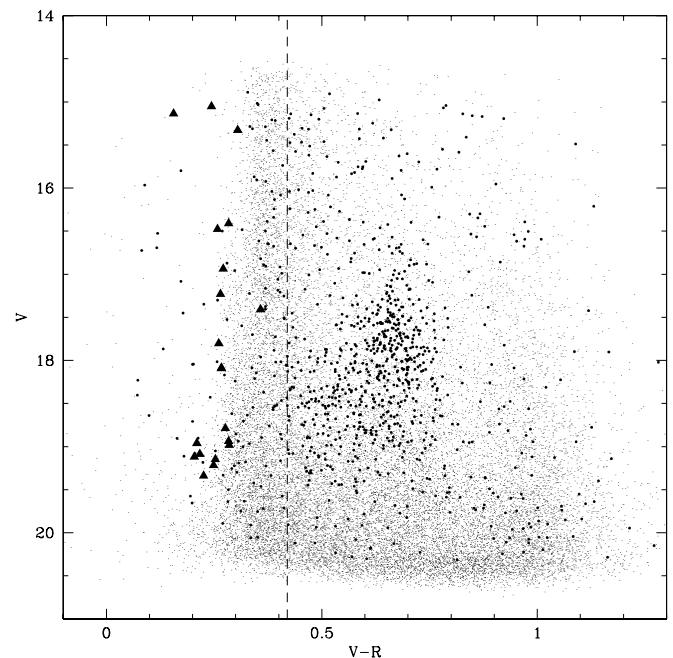


FIG. 6.—Color-magnitude diagram for a subsample of the data ($\sim 24,000$ stars in 8 deg^2). Variable stars are indicated with filled circles. Candidate RRLSs are located at the left of the dashed line. The triangles are the confirmed RRLSs. The sharp edge at $V-R \sim 0.3$ is the turnoff of the halo population.

calculated by using the LF algorithm (Lafleur & Kinman 1965), which works well even for a small number of observations. The criterion for the correct period is that the observations fall on a smooth curve when phased with this period. In other words, at the right period the sum of the squares of the magnitude difference between observations of adjacent phase has to be a minimum. Thus, for each trial period from 0.15 to 0.9 days, observations were sorted by increasing phase to calculate the parameter

$$\Theta = \frac{\sum_i (m_i - m_{i+1})^2}{\sum_i (m_i - \bar{m})^2}. \quad (2)$$

For each star, the minimum value of Θ gives the best period in the trial range. For aperiodic variables or stars with periods out of the range, this value has absolutely no meaning, and a plot of the light curve with the best period will show only noise. But for the RRLs, which have periods in this range, the light curves should look as expected for this type of variable.

To eliminate stars without periods in the trial range, we calculated the parameter Λ (Lafleur & Kinman 1965; Saha & Hoessel 1990):

$$\Lambda = \frac{\Theta \text{ (at incorrect period)}}{\Theta \text{ (at true period)}}, \quad (3)$$

where the true period is assumed to be the one that gives the minimum value of Θ and the average value of Θ over all the range of trial periods is adopted as the value of an incorrect period. After several tests with our data, we set a minimum requirement for Λ . Stars that had values of $\Lambda < 2.5$ at all trial periods were rejected from the list of candidate RRLs. The light curves of stars that had $\Lambda > 2.5$ were visually inspected, and RRLs were identified on the basis of their shapes (sawtooth for RRab and sinusoidal for RRc). For each star that passed the Λ threshold, we examined at least the three best periods (three lowest minima of Θ) in order to eliminate spurious periods that can arise from an external periodicity related to the time pattern of observation.

In Figure 7 we show an example of the period searching process for an RRab star. The star is one of the faintest in our sample ($\langle V \rangle = 19.75$), and it has only 14 observations. Consequently, it is more difficult to determine its period than the majority of the stars in our survey, which have been observed many more times and with greater precision. Even so, the figure shows that it is easy to identify the correct period of the star on the basis of the shape of its light curve.

Not surprisingly, we have found that the external period of 1 day, which is introduced by the way our observations were taken, has a large effect in the period search, producing two spurious periods (Π) at

$$\Pi^{-1} = P^{-1} \pm 1. \quad (4)$$

The spurious periods given by equation (4) also yield minima in Θ . For some stars, the light curves produced by these periods have essentially the same amount of noise as the ones given by what we believe are the true periods. The effect is particularly serious for RRc because both spurious periods may be within the range of typical periods for this type of

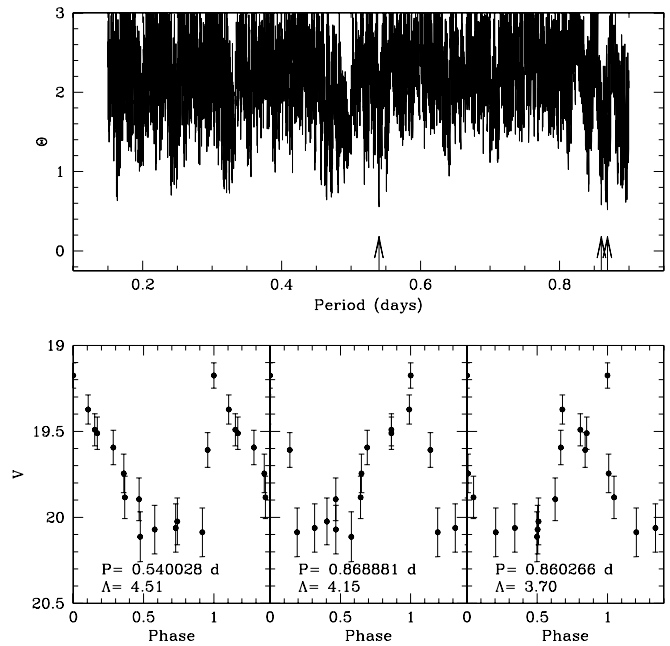


FIG. 7.—Example of the period-finding method for RR Lyrae 425, an RRab star near the faint limit of our survey. *Top*: Value of Θ for the trial periods. The arrows indicate the three minima selected. *Bottom*: Phased light curves with the three selected periods. Only the shortest period produces a light curve that has the shape expected of an RR Lyrae star.

star. An example of one of these cases is shown in Figure 8, which shows light curves for the three best periods found for one of our stars. All three curves look reasonably good for an RRc. We chose 0.3306 days as our best estimate of the period because it yields the largest value of Λ . However, a period of 0.2482 days (an alias of the first one) also produces a sinusoidal light curve. Thus, we cannot be certain which of the

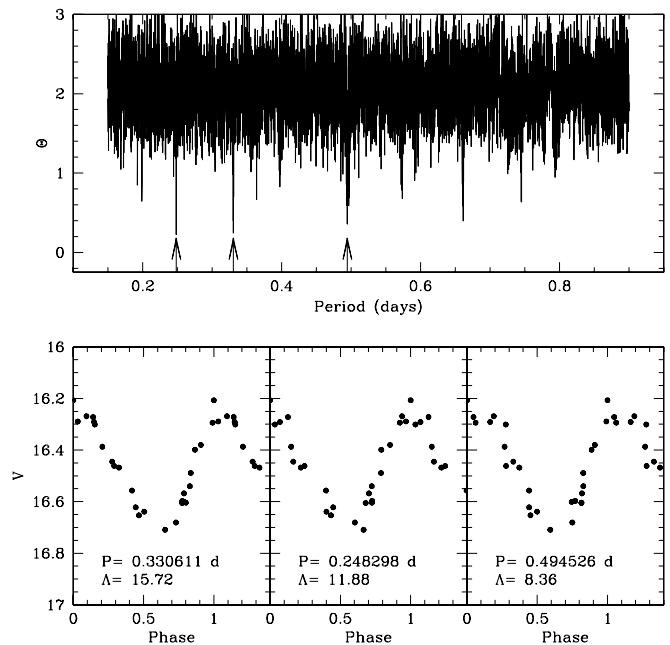


FIG. 8.—Same as Fig. 7, but for a moderately bright RRc. All three light curves look reasonably good for an RRc star. The period of 0.49 days is somewhat long for an RRc. In the catalog we report 0.33 days as our best estimate of the period, because it produces the largest value of Λ . However, we also list 0.25 days as a possible alternative.

two is the true period and which one is the alias. The third period in Figure 8 is discarded because is somewhat long for an RRc.

Sometimes with our data it is not possible to discriminate between the true period and a spurious one for the RRc stars. Since the typical periods of these stars range from 4 to 10 hr, it would be necessary to have observations with short time separations in order to isolate the true period. We are reporting as true period the one that produces the best light curve to the eye, which is frequently the one with the largest Λ value. However, if an acceptable light curve is produced by another period, it is also recorded in our catalog. This occurs in about 30% of the RRc stars. Consequently, the periods of the RRc variables that we report should be used with extreme caution in any analysis.

This problem is not serious for the RRab because the spurious periods produced by this effect are outside the typical range for this type of star. For example, a typical RRab star has a period of 0.539 days. The two spurious periods given by equation (4) are 0.350 and 1.169 days. The first one may be among one of the three lowest minima of Θ , but it will not be selected as the true period because it is too short for a sawtooth-type light curve; the latter is out of the range of all known RRLSs.

3.2. Light-Curve Fitting of RRab Stars

To measure precisely the amplitudes, times of maximum light, and the mean magnitudes of the RRab variables, we fitted template light curves from Layden (1998) to our observations. We tried six different templates with each star, which differed mainly in the slope of the rising branch of the light curve, and calculated for each fit three parameters using χ^2 minimization: amplitude, initial phase at maximum light, and magnitude at maximum light. One template was usually a better fit to the whole light curve than the others, and it was used to fix the time of maximum light and the star's mean magnitude, which was calculated by integrating the template light curve after it had been converted to intensity units. For the RRab variables, which in general have quite asymmetric light curves, this procedure is superior to a simple average of the observations, which is likely to produce mean magnitudes that are biased toward fainter values because more of the light cycle is spent fainter than mean light than brighter than it. This is much less of a problem in the case of the RRc, which have more symmetric light curves of smaller amplitude. For them, we adopted the average of our observations as the mean magnitude and estimated the times of maximum light and the amplitudes from the light curves given by our best estimates of their periods.

4. THE CATALOG

The final catalog contains 498 RRLSs, of which 395 (79%) are classified RRab and the remainder 103 as RRc. Table 2 contains right ascension (J2000.0); declination (J2000.0); the number of V observations in the light curve; V amplitude; period in days; a second possible period in some cases, as explained above; heliocentric Julian date at maximum light (HJD₀); type of RR Lyrae star; and the mean V magnitude with its error. The last column of the table has the name of the previously known RRLSs as given by the SIMBAD astronomical database.¹⁰

Electronic tables of the data for the individual light curves (Julian date, phase, V magnitude and error) are available upon request. Light curves of all RRLSs are shown in Figure 9. The solid line superimposed to the RRab stars is the best fit of a template to the observational data.

4.1. Completeness

The completeness of the survey depends on the available number of observations and the magnitude. Consequently, it varies with position on the sky. Even within the same region, the faintest stars usually have the fewest observations because their detection was more sensitive to bad seeing, atmospheric extinction, and brightness of the sky. The top panel of Figure 10 shows the mean number of observations for bright stars ($V < 18.5$) and faint ones ($V \geq 18.5$), as a function of right ascension.

To estimate the completeness of the survey, we have constructed artificial light curves and used them as input in our software to estimate how many are recovered as RRLSs. These simulations were done separately for RRab and RRc since the typical amplitudes and periods of these groups are quite different. The light curves were constructed using one of the templates in Layden (1998) for the RRab and a sine function for the RRc. For RRc, we chose random initial phases, amplitude, and periods. While all initial phases have equal chance of being picked, the periods and amplitudes were drawn from the distribution given by the known RRLSs in the GCVS. Those distributions can be approximated as Gaussian curves with means and standard deviations given in Table 3.

The case of RRab stars was treated differently since there is a known relationship between amplitude and period, in the sense that stars with larger amplitudes have shorter periods. There is, however, a large spread in this relationship. We estimated the size of the spread by using all stars in the GCVS

¹⁰ SIMBAD is operated at the Centre de Données Astronomique, Strasbourg, France.

TABLE 2
RR LYRAE STARS

ID	α (J2000.0)	δ (J2000.0)	N	Amp.	Period (days)	P_2 (days)	HJD ₀	Type	V	σV	Other Name
217.....	12 44 07.14	-00 56 48.7	36	0.31	0.394457	...	2,451,617.8334	<i>c</i>	16.34	0.02	...
218.....	12 44 29.71	-02 04 49.8	31	0.90	0.582238	...	2,45,1574.9038	<i>ab</i>	14.64	0.05	BU Vir
219.....	12 44 50.15	-00 50 39.4	34	0.43	0.247874	0.492859	2,451,643.7176	<i>c</i>	14.90	0.03	...
220.....	12 45 44.48	-01 53 26.5	31	0.55	0.587824	...	2,451,618.8402	<i>ab</i>	19.05	0.04	...
221.....	12 46 14.87	-01 03 11.6	28	1.12	0.521320	...	2,451,643.7321	<i>ab</i>	16.52	0.06	FASTT 553

NOTE.—Table 2 is presented in its entirety in the electronic edition of the Astronomical Journal. A portion is shown here for guidance regarding its form and content. Units of right ascension are hours, minutes, and seconds, and units of declination are degrees, arcminutes, and arcseconds.

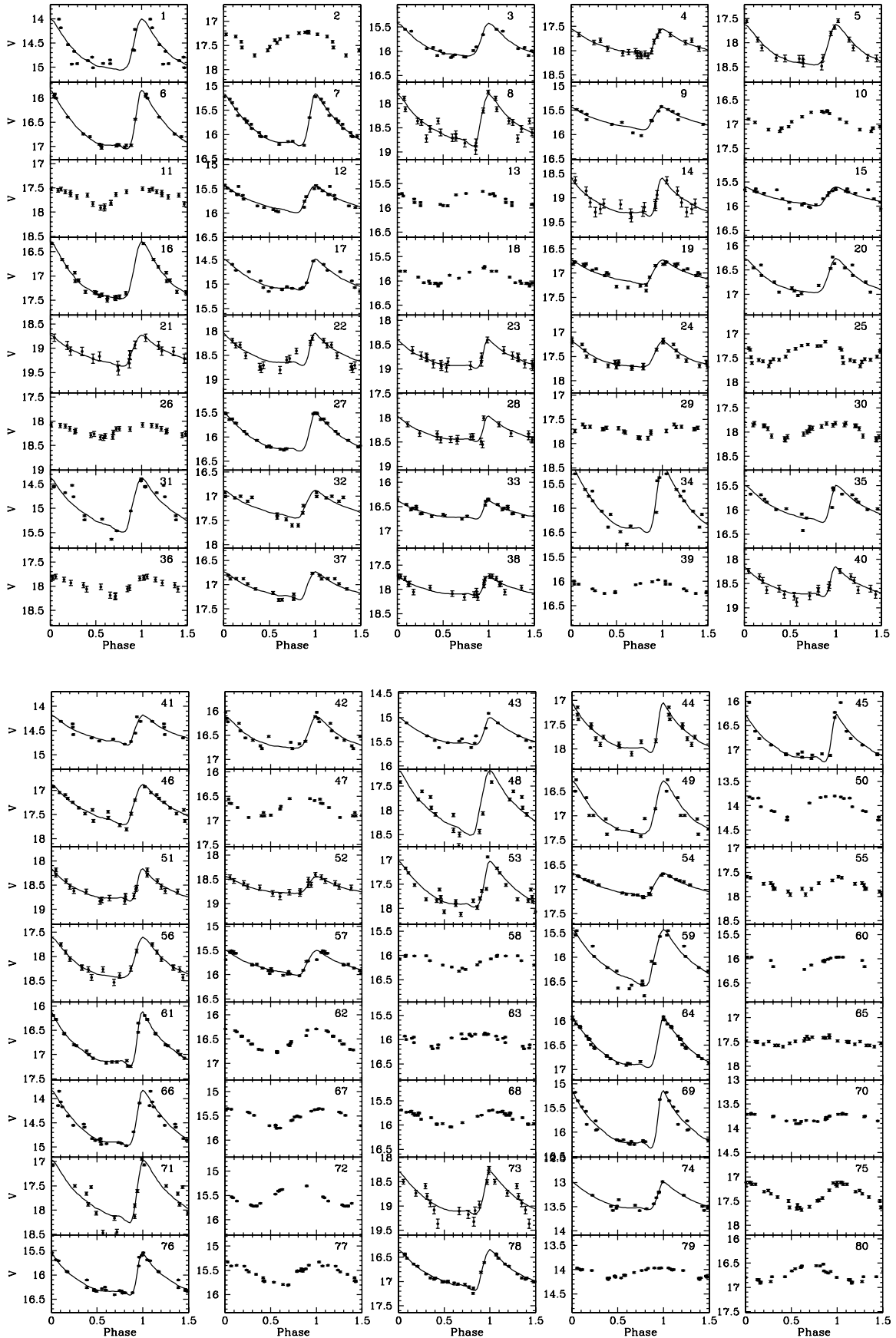


FIG. 9.—Light curves of the RRLSs. For RRab stars the best-fit templates are shown as solid lines.

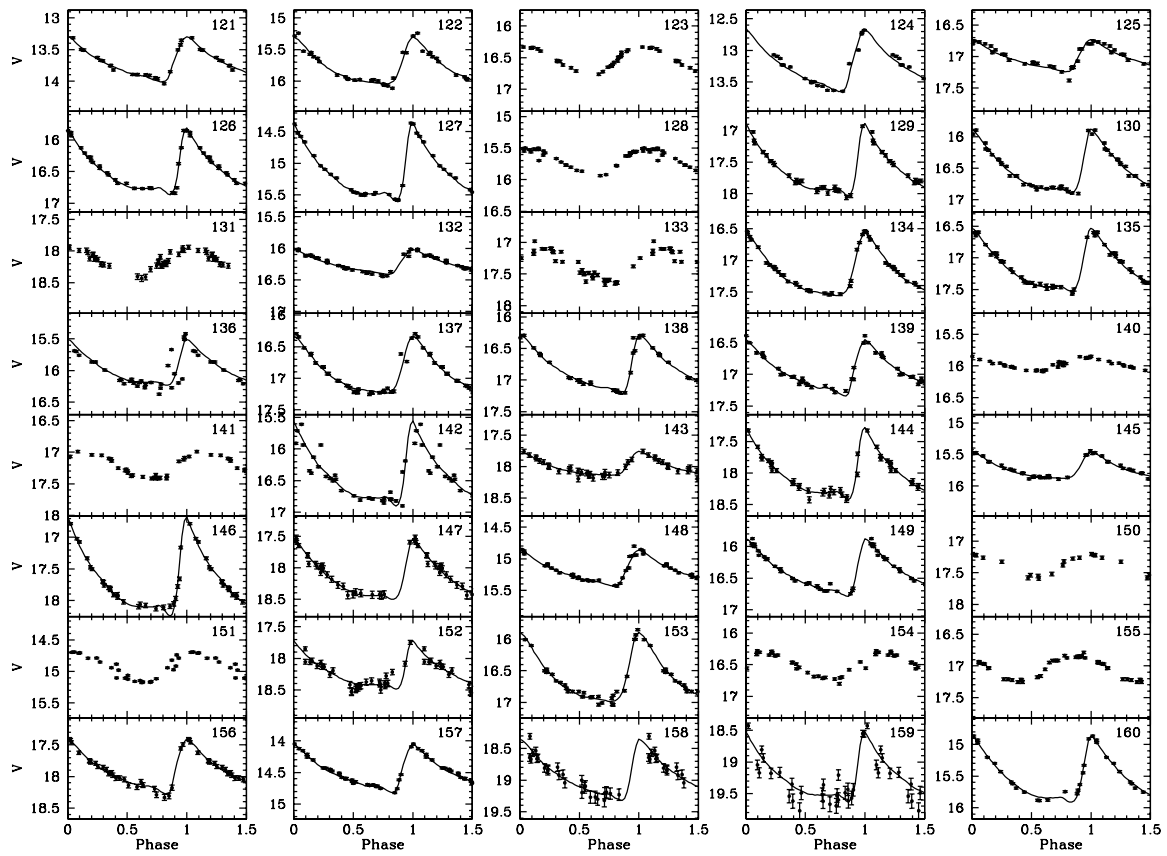
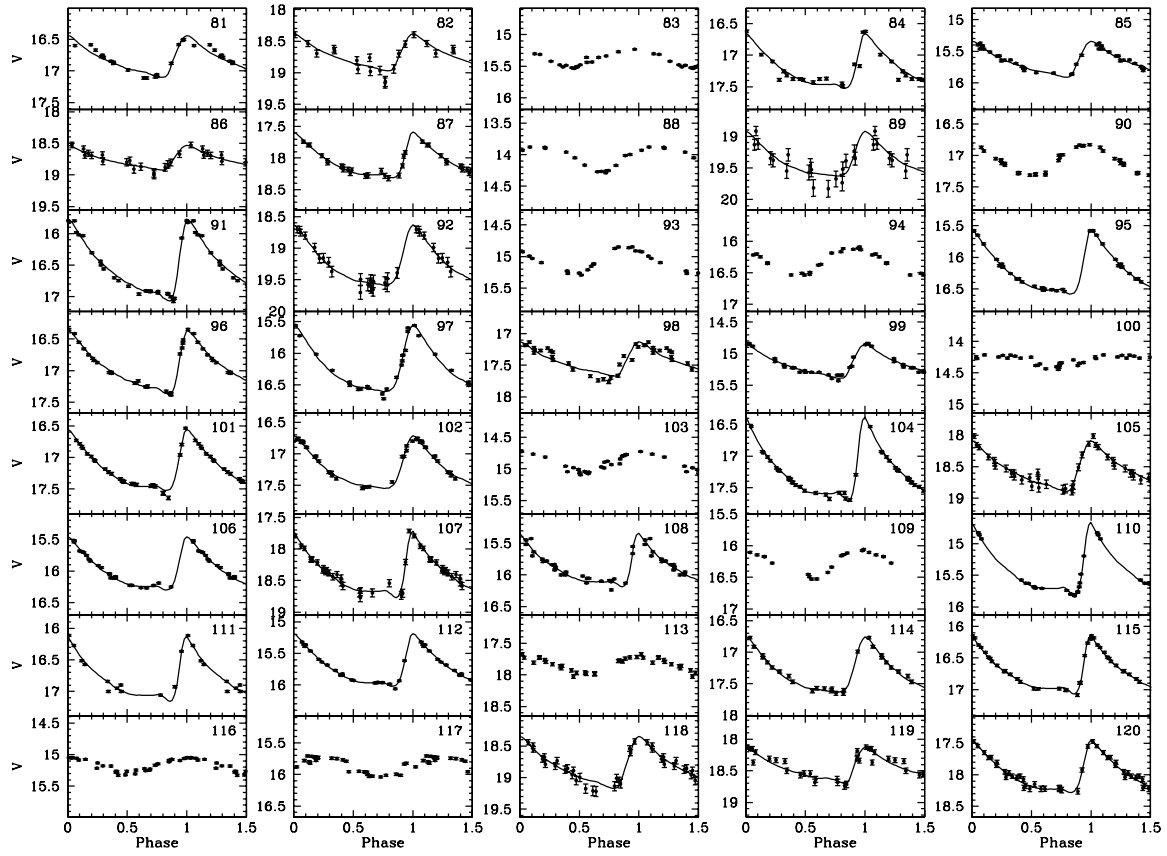


FIG. 9.—Continued

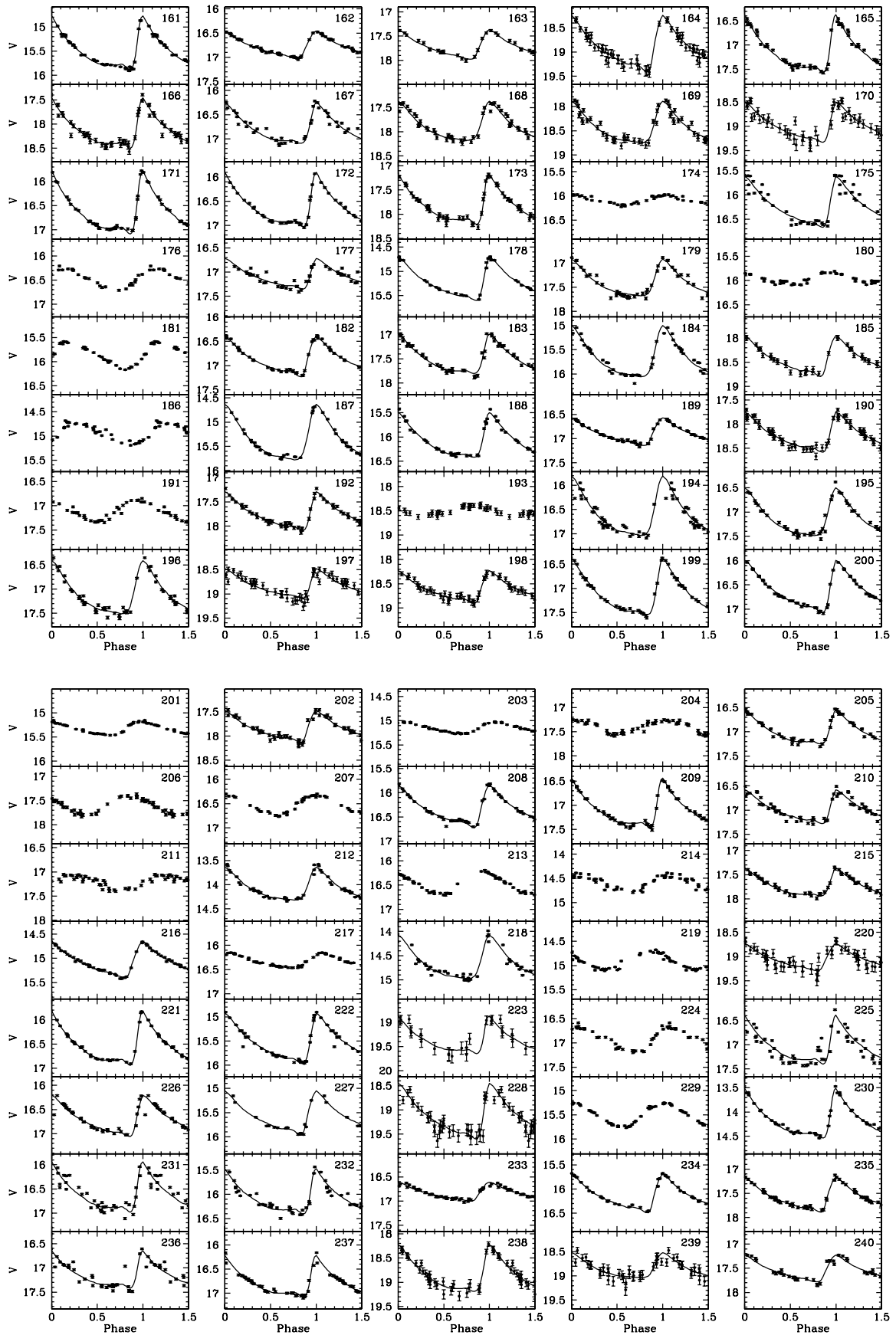


FIG. 9.—Continued

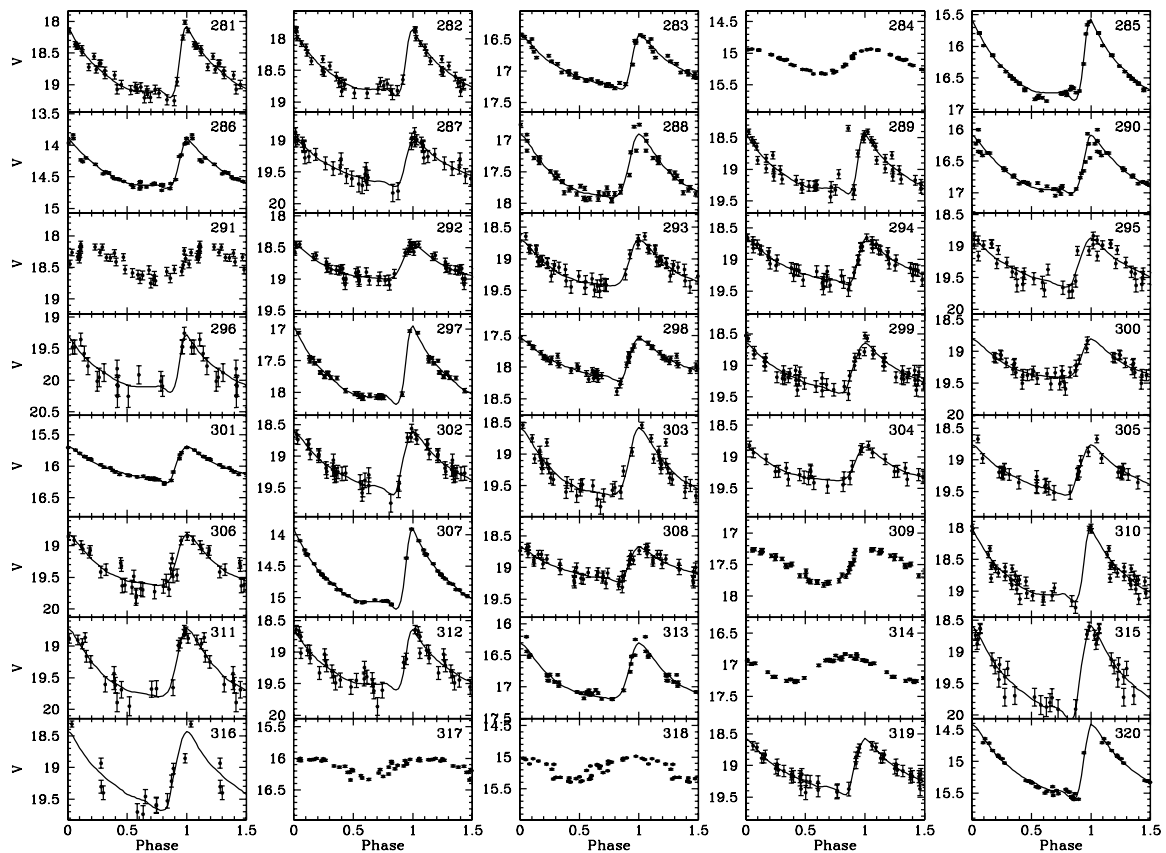
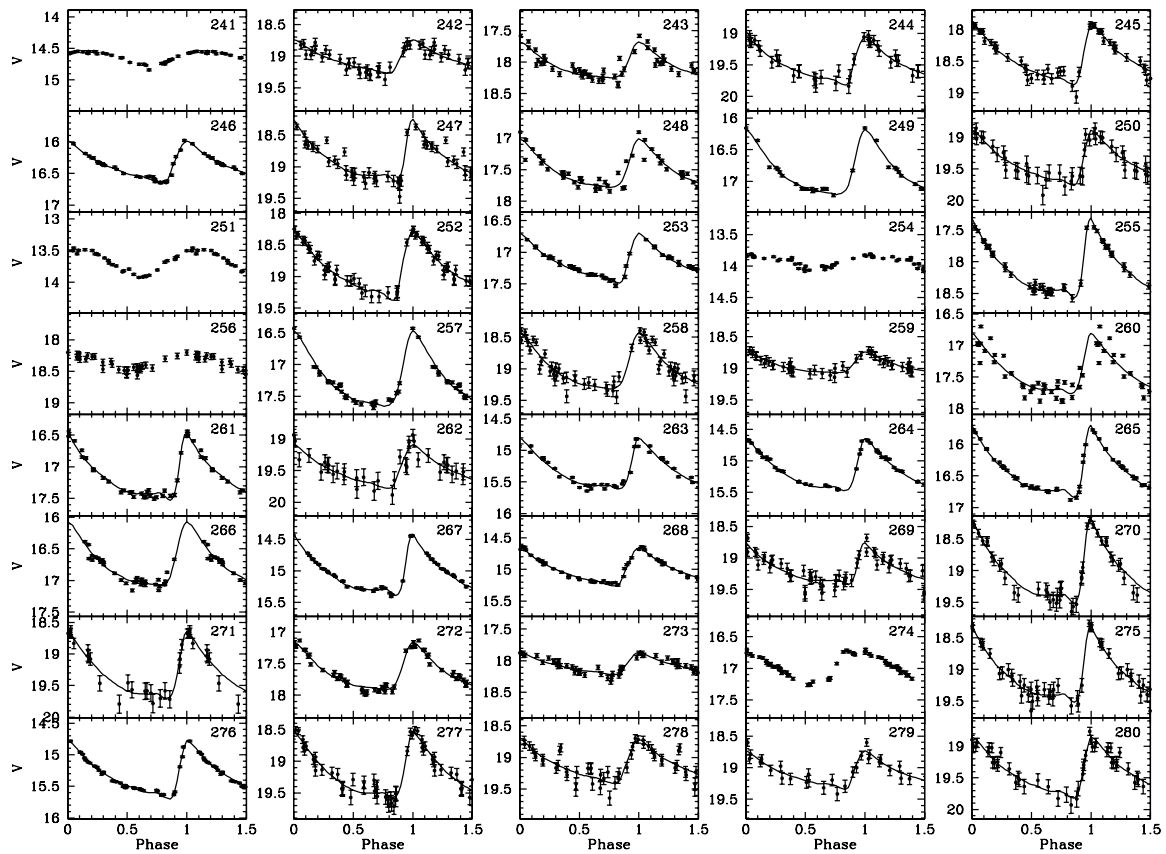


FIG. 9.—Continued

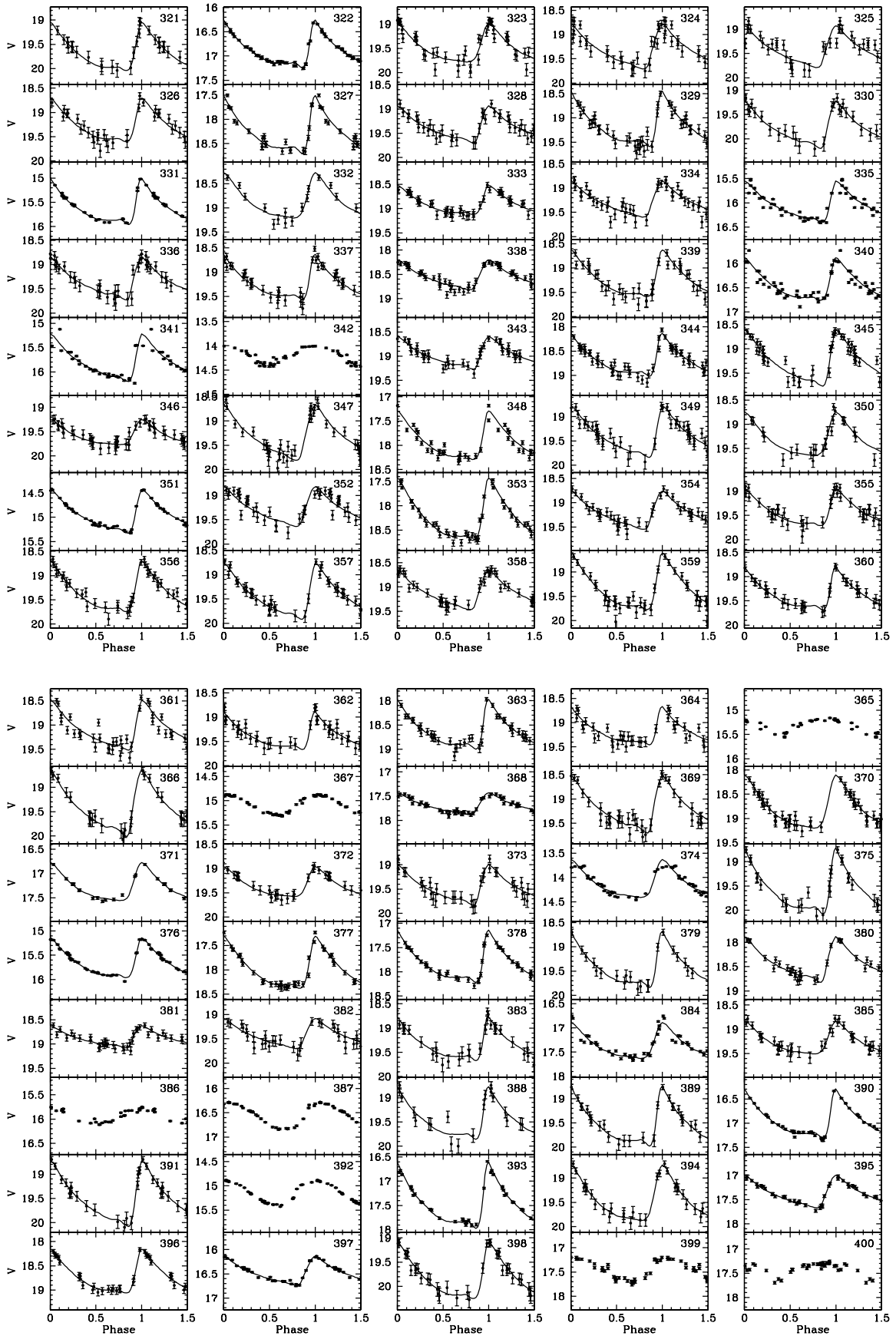


FIG. 9.—Continued

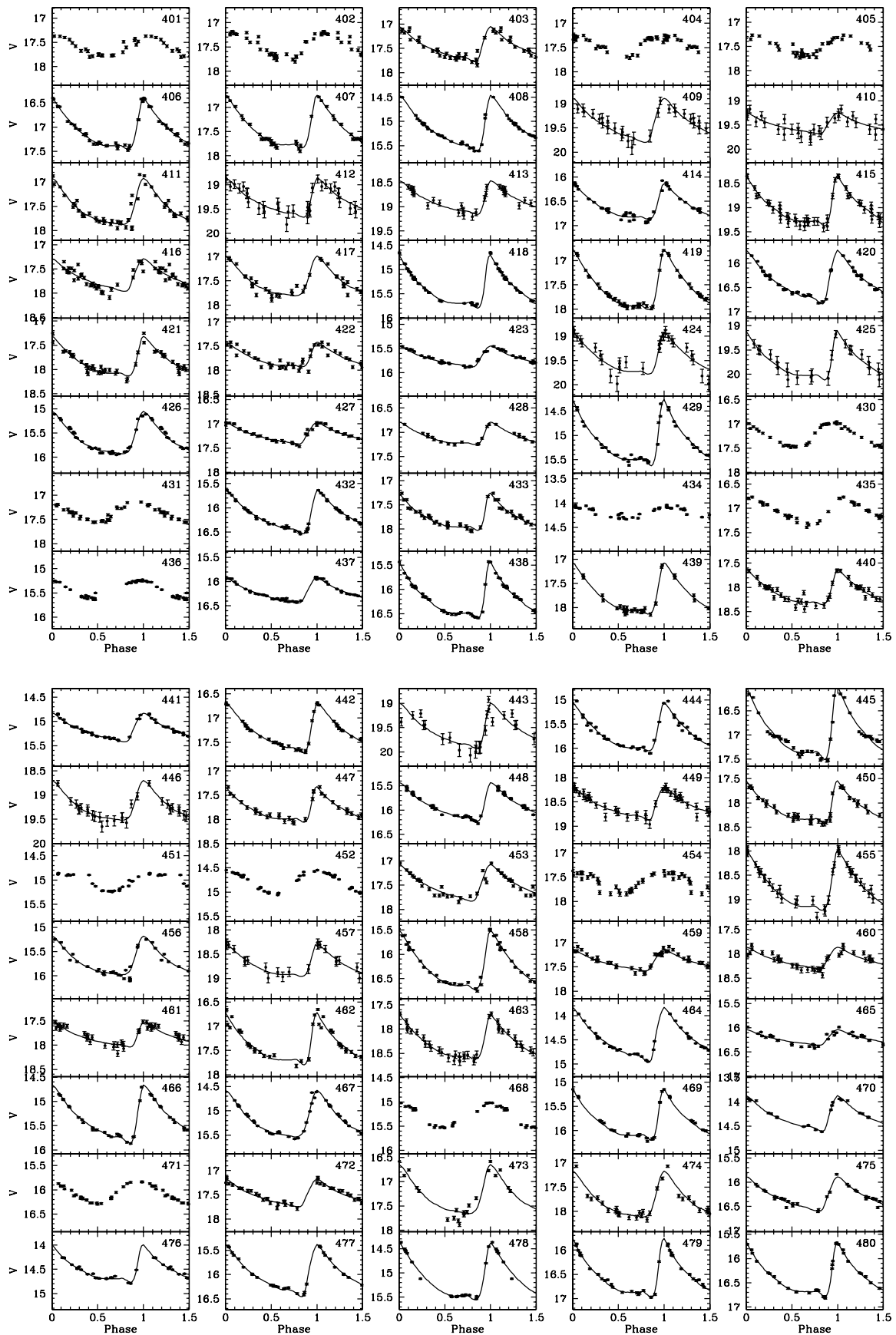


FIG. 9.—Continued

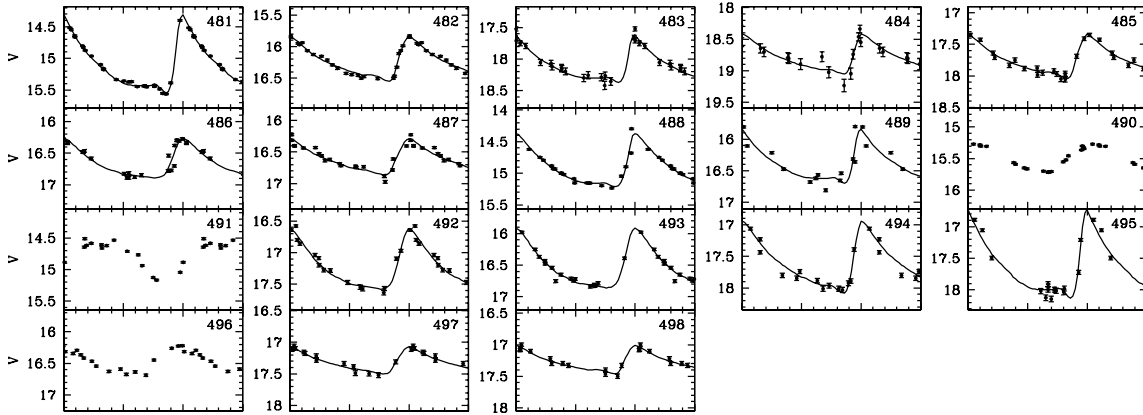


FIG. 9.—Continued

and calculating the difference in the logarithm of the period with respect to the one given by the period-amplitude relation of the globular cluster M3 (Siegel & Majewski 2000). Thus, for our simulated light curves, we picked a random amplitude from the GCVS distribution and selected a period from a distribution whose mean is the value given by the M3 relationship and standard deviation is of the size of the spread seen in the GCVS stars. The globular cluster M3 is the prototype of the Oosterhoff I group (OoI) of globular clusters. The use of this cluster as the center of our distribution of periods seems appropriate since most RRLs in the halo from the Lick survey are predominantly OoI stars (Suntzeff, Kinman, & Kraft 1991).

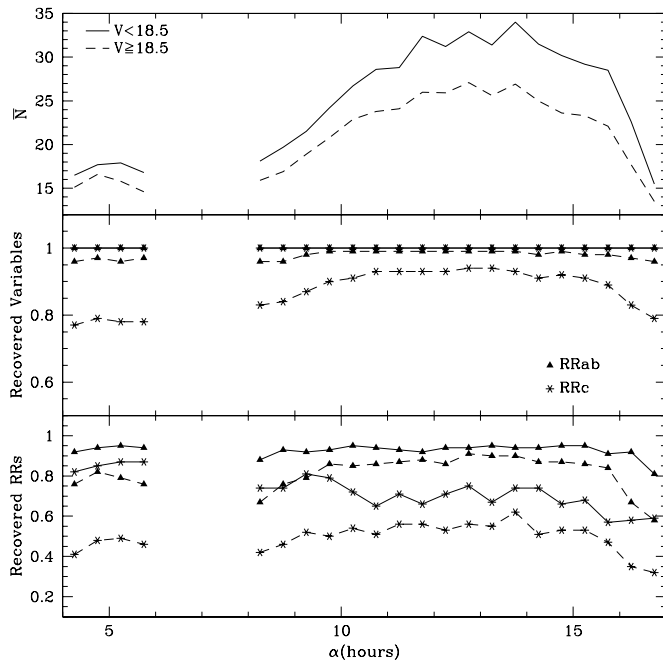


FIG. 10.—*Top*: Mean number of good measurements of each star along the observed region. *Middle*: Fraction of the artificial stars recovered as variables. *Bottom*: Fraction of the artificial stars recovered as RRs. In all panels the solid line indicates an average of the brightest stars ($V < 18.5$), and the dashed lines show the same quantity for the faintest objects. Triangles are RRab, and asterisks RRc stars.

For both RRab and RRc, we took the mean number of points and the times of observation from our real data in order to account for the actual phase coverage of our observations; these two items vary with right ascension. Finally, we introduced Gaussian noise to the artificial light curves to model our observational errors (Fig. 4).

In each region of the sky and in each 0.5 mag bin, from 14.0 to 20.0 in V , we calculated 1000 artificial RRLs and counted the number of stars we recovered as variable and the number of stars for which we obtained a period within 10% of the original value. The results were averaged for bright and faint stars and are shown in the lower panels of Figure 10. The simulations show that our software is able to recognize 100% of the bright artificial RRLs (both RRab and RRc) as variables. At the faint end of the survey there is a small chance that we miss some of the lower amplitude variables. Still, the fraction of recovered variables is high: greater than 96% for RRab and 77%–94% for RRc.

However, a star that is selected as variable is not necessarily recognized as an RRL. The phase coverage and the possibility of spurious periods play an important role in the process, especially for RRc stars. For bright stars, the total number of observations N does not change the results significantly. The completeness of the bright RRab stars remains at greater than 90% for most regions. Faint RRab stars are more sensitive to N . The completeness of RRc stars is lower and goes from 60%–90% for the brightest stars to 30%–60% for the faint ones. This, together with the fact that RRc variables are less common than RRab stars and that the number density of halo stars decreases exponentially with distance (hence magnitude), explains the relatively low number of faint RRc stars in our catalog.

These completeness estimates do not take into account objects that are blended with a nearby neighbor in our images. Such a blend may change the color of the object, and it may not pass our selection criteria. If the blend occurs only in the images with the worst seeing, the position of the star will not match among different scans and the number of observations for that star will be less than expected, maybe lower than our minimum requirement of $N = 12$. This effect is expected to be very low at high Galactic latitudes but is expected to increase when approaching the Galactic plane.

TABLE 3
PERIOD AND AMPLITUDE DISTRIBUTION OF RRLSs IN THE GCVS

TYPE	PERIOD (days)			V AMPLITUDE		
	N	Mean	σ	N	Mean	σ
<i>ab</i>	3884	0.539	0.09	300	1.04	0.24
<i>c</i>	365	0.335	0.07	46	0.536	0.13

The number of recovered RRLSs in the high-extinction region between $\alpha = 5^{\text{h}}1$ to 6^{h} in Figure 10 is only an upper limit to the true completeness. Because the extinction is highly patchy in this zone, it is not possible to modify appropriately the color criterion, and even without blends our completeness estimates may be systematically off.

4.2. Comparison with Other Catalogs

The vast majority of the stars in our list (429, or 86%) are new RRLSs. Only 15 of the stars in Table 2 are listed in the GCVS, seven of which are from the Lick survey of RRLSs (Kinman et al 1965, 1984) and will be discussed below. Of the remaining eight stars, only one, HN Vir, does not have a period in the GCVS. For it, we found a period of 0.575818 days. Our periods agree within 5×10^{-5} days for six of the seven stars with published periods. The remaining star is BS Vir, which, according to the GCVS, has a period of 0.3770874 days. This suggests that it is an RR*c*. Our period, 0.606415 days, produces an asymmetric light curve and amplitude that is typical of an RR*ab*. If our data are phased with the GCVS period, we still obtain an asymmetrical light curve, but with increased noise. We believe that the period in the GCVS is an alias and that the period found here is the correct one.

The Lick survey was carried out with photographic plates and has a limiting magnitude of $V \sim 16.5$. Our survey partially overlaps with Lick's field RR I [MWF 361A; $\alpha(\text{J2000.0}) = 16^{\text{h}}27^{\text{m}}25^{\text{s}}$, $\delta(\text{J2000.0}) = -3^{\circ}43'5''$]. Kinman et al. (1984) list 10 RRLSs in the region of overlap that are fainter than the saturation limit of our observations. We recovered successfully seven of these stars (five RR*ab* and two RR*c* stars), and our periods agree with the Lick survey to within 3×10^{-5} days. However, we failed to identify three stars: EH Ser, EM Ser, and V1041 Oph as RRLSs. All three stars were identified as variables in our survey and have the proper colors for RRLSs. However, for two, both RR*c* stars, we did not find a period in the expected range. Our completeness for RR*c* stars in this region is very low because of the small number of observations (see Fig. 10). The third is an RR*ab* star, but for it we had only 11 good measurements. Consequently, it was not included in the period search.

Our survey passes over the globular cluster Palomar 5. This cluster contains five RR*c* stars (Clement et al. 2001), and we recovered all of them (399=V1, 400=V2, 401=V5, 402=V4, and 404=V3). Although Pal 5 is a very loose cluster, the density of stars is significantly higher than in the general field. Our success in recovering every RRLS in this cluster indicates that our detection and photometry algorithms are adequate even in moderately crowded fields. The determination of periods of the Pal 5 RRLSs date back to Kinman & Rosino (1962). Our periods agree very well ($\Delta P = 3 \times 10^{-5}$ days) for Pal 5 V2 and V5. For the other three stars, we have found reciprocal periods that are the 1 day aliases of the original ones (eq. [4]). The periods reported by Kinman & Rosino (1962) are: 0.293230 days for Pal 5 V1, 0.329953 days for

Pal 5 V3, and 0.286362 days for Pal 5 V4, which are likely to be the correct ones because they are based on a larger number of observations, many of them taken during the same night. This confirms our suspicion that we could be reporting alias periods for some type *c* variables.

We have discovered two stars (403 and 405) that lie at $9'8''$ and $11'$ from the center of the cluster, respectively. Harris (1996) and Odenkirchen et al. (2002) report a tidal radius for this cluster of $\sim 16'$; however, other studies suggest that the tidal radius of this cluster has been overestimated and must have a size of $\sim 7'$ (Scholz et al. 1998; Leon, Meylan, & Combes 2000). Regardless of whether or not these stars are inside the tidal radius of the cluster, they are probably part of it because their mean V magnitudes (17.46 and 17.50) are identical with the mean magnitudes of the known RRLSs in Pal 5 ($V = 17.5 \pm 0.05$). As discussed in Vivas et al. (2001) and in more detail in Vivas & Zinn (2004), our survey has also detected several more distant variables that appear to be related to Pal 5.

Our survey confirms 49 of the RR Lyrae candidates that were identified by Ivezić et al. (2000). They searched for RRLSs using only two different epochs of the commissioning data of the SDSS. Their data go about 2 mag fainter than ours, and there is $\sim 50 \text{ deg}^2$ of overlap. We did not detect or have enough data to calculate periods for 13 of the faintest stars in their list. We were unable to find a period in the expected range for RRLSs for 13 other stars in their list. This is consistent with their sample having some degree of contamination from other types of blue variables and the incompleteness of our method, particularly for RR*c* variables. However, in the region of overlap, we also identified 132 RRLSs that were not recognized as candidates by the SDSS survey. Consequently, the completeness of the SDSS survey is 27%–34%, which is lower than the estimates given by Ivezić et al. (2000) and by our previous analysis of a smaller region of the sky (Vivas et al. 2001).

We have compared our list of RRLSs with the SIMBAD astronomical database and found that star 118 has been identified by Mateo, Fischer, & Krzemiński (1995) as an anomalous Cepheid in the Sextans dwarf spheroidal galaxy. They obtained a very similar period to the one we calculated from our data ($\Delta P = 9 \times 10^{-4}$ days). We did not detect the RRLSs in this galaxy because they are ~ 1 mag fainter than the limiting magnitude of our survey. Four of the RRLSs in our survey (367, 374, 478, and 488) were previously selected as having very low metal abundance from a HK objective prism survey (Norris, Ryan, & Beers 1999; Wilhelm et al. 1999). Sixty-one of our stars have already been detected as variable stars in the FASTT survey (Henden & Stone 1998), and 12 stars were observed in the 2dF quasar redshift survey (Croom et al. 2001) and classified as having a galactic star spectrum.

The above comparisons provide confidence that our techniques are successful at finding and determining the periods of the RRLSs, with the caveat that, as expected, they work less well for the RR*c* variables than for the RR*ab* ones and when a relatively small number of epochs have been observed. They also show that even with ample numbers of observations, the periods that we find for some RR*c* variables may be aliases.

4.3. Possible Contaminants

Anomalous Cepheids, pulsating blue stragglers and W UMa variables have photometric properties that sufficiently resemble

RRLSs that they could contaminate our sample. Some anomalous Cepheids can have periods of less than 0.9 days and colors and light curves that resemble type *b* RR Lyrae stars. A good example is the anomalous Cepheid in the Sextans dSph that we identified as an RRLS (see above). Because anomalous Cepheids are more luminous than RRLSs, they can be easily identified by their location in the color-magnitude diagram of a population of stars at the same distance (e.g., globular clusters or dSph galaxies). But it is very hard to recognize them in the field of the halo. Anomalous Cepheids have been found in every one of the Milky Way's dSph galaxies, and if the halo of the Galaxy was formed by the accretion of similar objects, we should expect it to have the same proportion of anomalous Cepheids to RRLSs as the dSph galaxies. The ratio between the number of anomalous Cepheids to RRLSs in dSph galaxies varies from 0.003 in Draco to 0.17 in Sextans (Mateo 1998). On average, for every 100 RRLSs there are ~ 3.5 anomalous Cepheids, but only half of them have periods less than 0.9 days (Nemec, Wehlau, & Mendes de Oliveira 1988) and can be confused with RRLSs. Therefore, if the halo resembles the dSph galaxies in the production of anomalous Cepheids, $\leq 2\%$ of the stars in our catalog are likely to be anomalous Cepheids. There is additional evidence that this source of contamination is small. Anomalous Cepheids are metal-poor stars that have roughly twice the mass of RRLSs. Their relatively large masses are either the result of mass transfer in binary systems (blue stragglers) or indicative of relatively young ages (Zinn & Searle 1976; Bono et al. 1997). In either case, their progenitors should be bluer than the main-sequence turnoff of a very old and metal-poor population. A color-magnitude diagram of our data, such as the one shown in Figure 6, shows a sharp contrast between the number of stars on each side of the color of the main-sequence turnoff of the halo. This "wall" indicates that the young stars or blue stragglers are a very small fraction of the very old stars. Since the likelihood that these young or blue straggler stars evolve to the anomalous Cepheid stage and the lifetime of the stage is not much different from the same parameters for RRLSs, the relative proportions of these main-sequence progenitors should be indicative of the ratio of anomalous Cepheids to RRLSs, which we conclude is very small.

Some blue straggler stars (BSSs) are themselves pulsating variables of the δ Scuti or SX Phe types. At the high Galactic latitudes of most of our survey, BSS belonging to the old disk population, which includes the δ Scuti variables, will be brighter than the bright cutoff of our survey and therefore not a source of contamination. This is not true for the region $5^{\text{h}}4 < \alpha < 6^{\text{h}}1$, which has $-20^\circ < b < -10^\circ$ and high extinction. The δ Scuti variables in this region and at all positions the SX Phe variables, which are BSS of the halo population, may have been detected as variable by our survey.

Few of the pulsating BSS are likely, however, to have been misidentified as RRLSs by passing all of our selection criteria. Although these stars will pass our color criterion, only a fraction will pass the amplitude one ($\Delta V > 0.2$). The catalogs of δ Scuti and SX Phe variables (Rodríguez, López-González, & López de Coca 2000; Rodríguez & López-González 2000) suggest that $\sim 35\%$ of these stars have amplitudes greater than this limit, but this may be an overestimate because the large amplitude variables are the easiest to detect. The very thorough study by Pych et al. (2001) of the globular cluster M55 revealed that $\sim 50\%$ of the BSS in the cluster are SX Phe pulsators, but only two of the 24 SX Phe stars have $\Delta V > 0.2$.

If M55 is representative of the Galactic halo, then only $\lesssim 5\%$ of the stars in the sparsely populated BSS region of the color-magnitude diagram (see Fig. 6) are expected to pass our amplitude criterion. The majority of those that do pass are likely to fail another selection criterion. Since the periods of the BSS pulsators are typically ≤ 0.1 days, they become a source of contamination for our survey only when a spurious period in the period range of the RRLSs produces a light curve that resembles the light curve of an RRLS. The light curve produced in this way is unlikely to match the period, amplitude, and shape that classifies the RR*ab*, but it is possible for one to resemble the lower amplitude, roughly sinusoidal light curve of an RR*c*. To estimate how frequently this may have occurred in our survey, we performed the following experiment. Since most of the contamination will be from SX Phe stars, we approximated one by a sinusoidal light curve of 0.06 days period, a V amplitude of 0.5, and a mean V magnitude of 17. Few SX Phe stars have such large amplitudes (Rodríguez & López-González 2000), but these are precisely the ones that can contaminate our survey. We constructed 20 artificial stars with these parameters, but with random epochs of maximum light. They were then "observed" at the same epochs and with the same photometric errors as our survey. Our period-finding software then attempted to find a period in the range of the RRLSs. The results depended on how many observations were made, which in our survey is a function of α (see Fig. 10). When there were more than 18 observations, none of these simulations produced a light curve remotely resembling that of an RRLS. With fewer than 18 observations, $\sim 5\%$ of the simulations produced a light curve that could be mistaken for an RR*c* with a period between 0.2 and 0.4 days. This suggests that among the 35 RR*c* our survey has found in the regions $4^{\text{h}}1 < \alpha < 6^{\text{h}}1$, $8^{\text{h}}0 < \alpha < 8^{\text{h}}5$, and $16^{\text{h}}5 < \alpha < 17^{\text{h}}0$, there may be a very small number of misidentified BSS pulsators; but in the better observed regions of the sky, this number is likely to be zero.

Another possible source of contamination for the RR*c* stars are the W UMa eclipsing binaries. When plotted with one-half of the binary period, the observations of some of these variables resemble the light curve of an RR*c* of that period. The color constraint that we placed on our survey rejects the majority of these variables. To match the apparent magnitude limits of our survey, the ones that pass the color criterion, which are on or near the main sequence, have to be members of the halo or thick disk populations. Because W UMa systems are rare compared with normal main-sequence stars, particularly the bluest ones (Mochneck 1985), and because the halo and the thick disk have low densities, probably few W UMa systems are included among the RR*c* variables in our survey.

5. SUMMARY

This survey has identified 498 RRLSs in a 380 deg^2 band of the sky. Most of these variables (86%) had not been identified previously. Our catalog contains the positions, mean magnitudes, and periods of the stars. For each star, the light curve that is produced by the period is presented. Simulations that use artificial light curves and model the frequencies of our observations indicate that the completeness of the survey is greater than 70% for the RR*ab* stars, but somewhat lower for the RR*c* variables (30%–90%, depending on the region of the sky). Very little contamination from other types of variables is expected because of the stringent limits that have been placed on amplitude, color, period, and light-curve shape.

The RRLs in our catalog span large ranges in Galactic latitude ($|b| = 10^\circ - 63^\circ$) and longitude ($l = 190^\circ - 18^\circ$) and lie 4–60 kpc from the Sun. They are therefore very valuable probes of the shape and density profile of the Galactic halo and the existence of substructure in the halo. These questions are examined in detail in Paper II of this series (Vivas & Zinn 2004). Some preliminary results may be found in Vivas & Zinn (2003), Vivas, Zinn, & Gallart (2003), and Zinn et al. (2003). The pulsational properties of the variables and their variation with position in the halo are discussed in the third paper to appear in this series.

The Llano del Hato Observatory is operated by CIDA for the Ministerio de Ciencia y Tecnología of Venezuela. This research project was partially supported by the National Science Foundation under grant AST 00-98428. Some funding was also provided by NSF's AST 99-87367 and grant S1-2001001144 of the Fondo Nacional de Ciencia y Tecnología of Venezuela. This paper constitutes part of the dissertation of A. K. V. to fulfill the requirements of the Ph.D. degree at Yale University. A. K. V. thanks Bruce Carney for several interesting and helpful comments and suggestions.

REFERENCES

- Akerlof, C., et al. 2000, *AJ*, 119, 1901
 Baltay, C., et al. 2002, *PASP*, 114, 780
 Briceño, C., et al. 2001, *Science*, 291, 93
 Bono, G., Caputo, F., Santolamazza, P., Cassisi, S., & Piersimoni, A. 1997, *AJ*, 113, 2209
 Catelan, M., Bellazzini, M., Landsman, W. B., Ferraro, F. R., Fusi Pecci, F., & Galletti, S. 2001a, *AJ*, 122, 3171
 Catelan, M., Ferraro, F. R., & Rood, R. T. 2001b, *ApJ*, 560, 970
 Chiba, M., & Beers, T. C. 2001, *ApJ*, 549, 325
 Clement, C. M., et al. 2001, *AJ*, 122, 2587
 Croom, S. M., Smith, R. J., Boyle, B. J., Shanks, T., Loring, N. S., Miller, L., & Lewis, I. J. 2001, *MNRAS*, 322, L29
 Dohm-Palmer, R. C., et al. 2001, *ApJ*, 555, L37
 Eggen, O. J., Lynden-Bell, D., & Sandage, A. R. 1962, *ApJ*, 136, 748
 Freeman, K., & Bland-Hawthorn, J. 2002, *ARA&A*, 40, 487
 Gilmore, G., Wyse, R. F. G., & Norris, J. E. 2002, *ApJ*, 574, L39
 Harris, W. E. 1996, *AJ*, 112, 1487
 Hawkins, M. R. S. 1984, *MNRAS*, 206, 433
 Henden, A. A., & Stone, R. C. 1998, *AJ*, 115, 296
 Ibata, R., Irwin, M., Lewis, G., Ferguson, A. M. N., & Tanvir, N. 2001a, *Nature*, 412, 49
 Ibata, R., Lewis, G. F., Irwin, M., Totten, E., & Quinn, T. 2001b, *ApJ*, 551, 294
 Ivezić, Z., et al. 2000, *AJ*, 120, 963
 Kholopov, P. N., et al. 1998, *The Combined General Catalogue of Variable Stars*, 4.1 Ed.
 Kinman, T. D., Mahaffey, C. T., & Wirtanen, C. A. 1982, *AJ*, 87, 314
 Kinman, T. D., & Rosino, L. 1962, *PASP*, 74, 499
 Kinman, T. D., Wirtanen, C. A., & Janes, K. A. 1965, *ApJS*, 11, 223
 ———. 1966, *ApJS*, 13, 379
 Kinman, T. D., Wong-Swanson, B., Wenz, M., & Harlan, E. A. 1984, *AJ*, 89, 1200
 Laffer, J., & Kinman, T. D. 1965, *ApJS*, 11, 216
 Landolt, A. U. 1983, *AJ*, 88, 439
 Layden, A. C. 1998, *AJ*, 115, 193
 Lejeune, T., Cuisinier, F., & Buser, R. 1998, *A&AS*, 130, 65
 Leon, S., Meylan, G., & Combes, F. 2000, *A&A*, 359, 907
 Majewski, S. R. 1993, *ARA&A*, 31, 575
 Majewski, S. R., Skrutskie, M. F., Weinberg, M. D., & Ostheimer, J. C. 2003, *ApJ*, 592, 1082
 Mateo, M. 1998, *ARA&A*, 36, 435
 Mateo, M., Fischer, P., & Krzemiński, W. 1995, *AJ*, 110, 2166
 Mochnacki, S. W. 1985, in *Interacting Binaries* (Dordrecht: Reidel), 51
 Monet, D., et al. 1998, in *The PMM USNO-A2.0 Catalog* (Washington: USNO)
 Nemeč, J. M., Wehlau, A., & Mendes de Oliveira, C. 1988, *AJ*, 96, 528
 Newberg, H. J., et al. 2002, *ApJ*, 569, 245
 Norris, J. E. 1994, *ApJ*, 431, 645
 Norris, J. E., Ryan, S. G., & Beers, T. C. 1999, *ApJS*, 123, 639
 Odenkirchen, M., Grebel, E. K., Dehnen, W., Rix, H.-W., & Cudworth, K. M. 2002, *AJ*, 124, 1497
 Peng, E. W., Ford, H. C., Freeman, K. C., & White, R. L. 2002, *AJ*, 124, 3144
 Plaut, L. 1966, *Bull. Astron. Inst. Netherlands Suppl.*, 1, 105
 ———. 1968, *Bull. Astron. Inst. Netherlands Suppl.*, 2, 293
 ———. 1971, *A&AS*, 4, 75
 Press, W. H., Teukolsky, S. A., Vetterling, W. T., & Flannery, B. P. 1992, *Numerical Recipes in C* (2d ed; Cambridge Univ. Press)
 Pych, W., Kaluzny, J., Krzemiński, W., Schwarzenberg-Czerny, A., & Thompson, I. B. 2001, *A&A*, 367, 148
 Rey, S.-C., Yoon, S.-J., Lee, Y.-W., Chaboyer, B., & Sarajedini, A. 2001, *AJ*, 122, 3219
 Rodríguez, E., & López-González, M. J. 2000, *A&A*, 359, 597
 Rodríguez, E., López-González, M. J., & López de Coca, P. 2000, *A&AS*, 144, 469
 Sabbey, C. N., Coppi, P., & Oemler, A. 1998, *PASP*, 110, 1067
 Saha, A. 1985, *ApJ*, 289, 310
 Saha, A., & Hoessel, J. G. 1990, *AJ*, 99, 97
 Schlegel, D. J., Finkbeiner, D. P., & Davis, M. 1998, *ApJ*, 500, 525
 Scholz, R.-D., Irwin, M., Odenkirchen, M., & Meusinger, H. 1998, *A&A*, 333, 531
 Searle, L., & Zinn, R. 1978, *ApJ*, 225, 357
 Siegel, M. H., & Majewski, S. R. 2000, *AJ*, 120, 284
 Smith, H. A. 1995, *RR Lyrae Stars* (Cambridge: Cambridge Univ. Press)
 Suntzeff, N. B., Kinman, T., & Kraft, R. P. 1991, *ApJ*, 367, 528
 Vivas, A. K., et al. 2001, *ApJ*, 554, L33
 Vivas, A. K., & Zinn, R. 2003, *Mem. Soc. Astron. Italiana*, 74, 928
 ———. 2004, in preparation (Paper II)
 Vivas, A. K., Zinn, R., & Gallart, C. 2003, in *ASP Conf. Ser., Satellite and Tidal Streams*, ed. F. Prada, D. Martínez-Delgado, & T. Mahoney (San Francisco: ASP), in press
 Wetterer, C. J., & McGraw, J. T. 1996, *AJ*, 112, 1046
 Wetterer, C. J., McGraw, J. T., Hess, T. R., & Grashuis, R. 1996, *AJ*, 112, 742
 Wilhelm, R., Beers, T. C., Sommer-Larsen, J., Pier, J. R., Layden, A. C., Flynn, C., Rossi, S., & Christensen, P. R. 1999, *AJ*, 117, 2329
 Yanny, B., et al. 2000, *ApJ*, 540, 825
 ———. 2003, *ApJ*, 588, 824
 Zinn, R. 1993, in *ASP Conf. Ser. 48, The Globular Cluster-Galaxy Connection*, ed. G. H. Smith & J. P. Brodie (San Francisco: ASP), 38
 Zinn, R., & Searle L. 1976, *ApJ*, 209, 734
 Zinn, R., Vivas, A. K., Gallart, C., & Winnick, R. 2003, in *ASP Conf. Ser., Satellite and Tidal Streams*, ed. F. Prada, D. Martínez-Delgado, & T. Mahoney (San Francisco: ASP), in press